AD-A046 804 NAVAL RESEARCH LAB WASHINGTON D C F/G 17/1
HYDROPHONE SENSOR HAVING A CARDIOID DIRECTIVITY PATTERN.(U)
JUL 77 G D HUGUS

UNCLASSIFIED NRL-MR-3565 SBIE-AD-E000 013 NL

| OF |
ADA046804

END
DATE FILMED
12-77
DDC

AD-E000013

AD A046804

NRL Memorandum Report 3565

Hydrophone Sensor Having a Cardioid Directivity Pattern.

G. D. Hugus III

Standards Branch
Underwater Sound Reference Division
P.O. Box 8337, Orlando, Florida 32806

Final rept. 10 Apr 75-29 Mar 77,

NRL-MR-3565

July 1977

22 p.

F11121

ZF11121003

SBIE

AD-E000013

DDC
RECEIVED
NOV 23 1977
B

NAVAL RESEARCH LABORATORY
Washington, D.C.

Approved for public release; distribution unlimited

AD No.
DDC FILE COPY

251 950

-- 1 - AD NUMBER: E000013

-- 2 - FIELDS AND GROUPS: 9/1, 17/1

-- 3 - CATALOG CARD CLASSIFICATION: UNCLASSIFIED

-- 4 - PRICES:

-- 5 - CORPORATE AUTHOR: NAVAL RESEARCH LAB WASHINGTON
-- D C

-- 6 - UNCLASSIFIED TITLE: HYDROPHONE SENSOR HAVING
-- A CARDIOID DIRECTIVITY PATTERN.

-- 7 - CLASSIFIED TITLE:

-- 8 - TITLE CLASSIFICATION: UNCLASSIFIED

-- 9 - DESCRIPTIVE NOTE: FINAL REPT. 10 APR 75-29 MAR 77,

--10 - PERSONAL AUTHORS: HUGUS,G. DICKSON ,III;

--11 - REPORT DATE: JUL , 1977

--12 - PAGINATION: 21P

--14 - REPORT NUMBER: NRL-MR-3565

--15 - CONTRACT NUMBER:

--16 - PROJECT NUMBER: F11121

--17 - TASK NUMBER: ZF11121003

--18 - MONITOR ACRONYM:

--19 - MONITOR SERIES:

--20 - REPORT CLASSIFICATION: UNCLASSIFIED

--21 - SUPPLEMENTARY NOTE:

--22 - LIMITATIONS (ALPHA): DISTRIBUTION OF DOCUMENT
-- CONTROLLED BY NAVAL RESEARCH LABORATORY, ATTN:
-- CODE 2628, WASHINGTON, D.C. 20375. THIS DOCUMENT
-- IS NOT AVAILABLE FROM DDC. CATALOGING INFORMATION
-- SUPPLIED BY NRL.

--23 - DESCRIPTORS: *HYDROPHONES, *ELECTROACOUSTICS,
-- *DETECTORS, OMNIDIRECTIONAL, CONFIGURATIONS,
-- SENSITIVITY

--24 - DESCRIPTOR CLASSIFICATION: UNCLASSIFIED

--25 - IDENTIFIERS: *HYDROPHONE SENSOR, *CARDIOID
-- DIRECTIVITY PATTERN, USRD H73, PE62711N, WUS02-36

--26 - IDENTIFIER CLASSIFICATION: UNCLASSIFIED

--27 - ABSTRACT: THE ELECTROACOUSTIC ANALYSIS IS
-- PRESENTED TOGETHER WITH ACTUAL ACOUSTIC
-- PERFORMANCE OF A HYDROPHONE SENSOR CONFIGURATION
-- THAT IS OMNIDIRECTIONAL BELOW ITS HORIZONTAL
-- PLANE AND HAVING REDUCED SENSITIVITY ABOVE THIS
-- PLANE. THIS SENSOR IS INHERENTLY OMNIDIRECTIONAL
-- IN THE HORIZONTAL PLANE. THE SENSOR CONSISTS OF
-- AN AXIALLY POLLED PIEZO-CERAMIC TUBE WITH PISTONS
-- OF DIFFERENT MASSES CEMENTED TO EACH END. THIS
-- ASSEMBLE IS MOUNTED WITH AXIS VERTICAL INSIDE AN
-- AIR FILLED TUBULAR CERAMIC HOUSING SO THAT ONLY
-- THE PISTON OUTSIDE FACES ARE EXPOSED TO THE SOUND
-- PRESSURE. THE EQUATIONS ARE DERIVED FOR THE
-- THEORETICAL VERTICAL DIRECTIVITY OF THE SENSOR

-- AS A FUNCTION OF VERTICAL ANGLE, PISTON DYNAMIC
-- MASS RATIO, PISTON RADIUS, AND SENSOR AXIAL
-- LENGTH PARAMETERS.

--28 - ABSTRACT CLASSIFICATION: UNCLASSIFIED

--29 - INITIAL INVENTORY: XXXXX

--30 - ANNOTATION:

--31 - SPECIAL INDICATOR:

--32 - REGRADE CATEGORY:

--33 - LIMITATION CODES: 1 21

--34 - SOURCE SERIES: F

--35 - SOURCE CODE: 251950

--36 - DOCUMENT LOCATION: NRL

--37 - CLASSIFICATION AUTHORITY:

--38 - DECLASSIFICATION DATE:

--39 - DOWNGRADING DATE:

--40 - GEOPOLITICAL CODE: 1100

-- 5 - CORPORATE AUTHOR: NAVAL RESEARCH LAB WASHINGTON
-- D C
-- 6 - UNCLASSIFIED TITLE: HYDROPHONE SENSOR HAVING
-- A CARDIOID DIRECTIVITY PATTERN.
-- 7 - CLASSIFIED TITLE:
-- 8 - TITLE CLASSIFICATION: UNCLASSIFIED
-- 9 - DESCRIPTIVE NOTE: FINAL REPT. 10 APR 75-29 MAR 77,
--10 - PERSONAL AUTHORS: HUGUS,G. DICKSON ,III;
--11 - REPORT DATE: JUL , 1977
--12 - PAGINATION: 21P
--14 - REPORT NUMBER: NRL-MR-3565
--15 - CONTRACT NUMBER:
--16 - PROJECT NUMBER: F11121
--17 - TASK NUMBER: ZF11121003
--18 - MONITOR ACRONYM:
--19 - MONITOR SERIES:
--20 - REPORT CLASSIFICATION: UNCLASSIFIED
--21 - SUPPLEMENTARY NOTE:
--22 - LIMITATIONS (ALPHA): DISTRIBUTION OF DOCUMENT
-- CONTROLLED BY NAVAL RESEARCH LABORATORY, ATTN:
-- CODE 2628, WASHINGTON, D.C. 20375. THIS DOCUMENT
-- IS NOT AVAILABLE FROM DDC. CATALOGING INFORMATION
-- SUPPLIED BY NRL.
--23 - DESCRIPTORS: *HYDROPHONES, *ELECTROACOUSTICS,
-- *DETECTORS, OMNIDIRECTIONAL, CONFIGURATIONS,
-- SENSITIVITY
--24 - DESCRIPTOR CLASSIFICATION: UNCLASSIFIED
--25 - IDENTIFIERS: *HYDROPHONE SENSOR, *CARDIOID
-- DIRECTIVITY PATTERN, USRD H73, PE62711N, WUS02-36
--26 - IDENTIFIER CLASSIFICATION: UNCLASSIFIED
--27 - ABSTRACT: THE ELECTROACOUSTIC ANALYSIS IS
-- PRESENTED TOGETHER WITH ACTUAL ACOUSTIC
-- PERFORMANCE OF A HYDROPHONE SENSOR CONFIGURATION
-- THAT IS OMNIDIRECTIONAL BELOW ITS HORIZONTAL
-- PLANE AND HAVING REDUCED SENSITIVITY ABOVE THIS
-- PLANE. THIS SENSOR IS INHERENTLY OMNIDIRECTIONAL
-- IN THE HORIZONTAL PLANE. THE SENSOR CONSISTS OF
-- AN AXIALLY POLLED PIEZO-CERAMIC TUBE WITH PISTONS
-- OF DIFFERENT MASSES CEMENTED TO EACH END. THIS
-- ASSEMBLE IS MOUNTED WITH AXIS VERTICAL INSIDE AN
-- AIR FILLED TUBULAR CERAMIC HOUSING SO THAT ONLY
-- THE PISTON OUTSIDE FACES ARE EXPOSED TO THE SOUND
-- PRESSURE. THE EQUATIONS ARE DERIVED FOR THE
-- THEORETICAL VERTICAL DIRECTIVITY OF THE SENSOR

-- AS A FUNCTION OF VERTICAL ANGLE, PISTON DYNAMIC
-- MASS RATIO, PISTON RADIUS, AND SENSOR AXIAL
-- LENGTH PARAMETERS.
--28 - ABSTRACT CLASSIFICATION: UNCLASSIFIED
--29 - INITIAL INVENTORY: XXXXX
--30 - ANNOTATION:
--31 - SPECIAL INDICATOR:
--32 - REGRADE CATEGORY:
--33 - LIMITATION CODES: 1 21
--34 - SOURCE SERIES: F
--35 - SOURCE CODE: 251950
--36 - DOCUMENT LOCATION: NRL
--37 - CLASSIFICATION AUTHORITY:
--38 - DECLASSIFICATION DATE:
--39 - DOWNGRADING DATE:
--40 - GEOPOLITICAL CODE: 1100
--41 - TYPE CODE: N
--42 - IAC ACCESSION NUMBER:
--43 - IAC DOCUMENT TYPE:
--44 - IAC SUBJECT TERMS:

2

SECURITY CLASSIFICATION OF THIS PAGE (When Data Entered)

REPORT DOCUMENTATION PAGE		READ INSTRUCTIONS BEFORE COMPLETING FORM
1. REPORT NUMBER NRL Memorandum Report 3565	2. GOVT ACCESSION NO.	3. RECIPIENT'S CATALOG NUMBER
4. TITLE (and Subtitle) HYDROPHONE SENSOR HAVING A CARDIOID DIRECTIVITY PATTERN		5. TYPE OF REPORT & PERIOD COVERED Final Report - 10 April 1975 to 29 March 1977 6. PERFORMING ORG. REPORT NUMBER
7. AUTHOR(s) G. Dickson Hugus III		8. CONTRACT OR GRANT NUMBER(s)
9. PERFORMING ORGANIZATION NAME AND ADDRESS Naval Research Laboratory Underwater Sound Reference Division P.O. Box 8337, Orlando, Florida 32806		10. PROGRAM ELEMENT, PROJECT, TASK AREA & WORK UNIT NUMBERS NRL Problem SO2-36 and 31 62711N ZF-11-121-003
11. CONTROLLING OFFICE NAME AND ADDRESS		12. REPORT DATE July 1977 13. NUMBER OF PAGES 21
14. MONITORING AGENCY NAME & ADDRESS(if different from Controlling Office)		15. SECURITY CLASS. (of this report) Unclassified 15a. DECLASSIFICATION/DOWNGRADING SCHEDULE

16. DISTRIBUTION STATEMENT (of this Report)

Approved for public release; distribution unlimited.

17. DISTRIBUTION STATEMENT (of the abstract entered in Block 20, if different from Report)

18. SUPPLEMENTARY NOTES

19. KEY WORDS (Continue on reverse side if necessary and identify by block number)

Hydrophone Sensor
USRD type H73
Cardioid directivity pattern

20. ABSTRACT (Continue on reverse side if necessary and identify by block number)

The electroacoustic analysis is presented together with actual acoustic performance of a hydrophone sensor configuration that is omnidirectional below its horizontal plane and having reduced sensitivity above this plane. This sensor is inherently omnidirectional in the horizontal plane. The sensor consists of an axially polled piezo-ceramic tube with pistons of different masses cemented to each end. This assembly is mounted with axis vertical inside an air filled tubular ceramic housing so that only the piston outside faces are exposed to the sound pressure.

DD FORM 1 JAN 73 1473 EDITION OF 1 NOV 65 IS OBSOLETE
S/N 0102-014-6601

SECURITY CLASSIFICATION OF THIS PAGE (When Data Entered)

20. Abstract (Continued)

The equations are derived for the theoretical vertical directivity of the sensor as a function of vertical angle, piston dynamic mass ratio, piston radius, and sensor axial length parameters. A true cardioid directivity pattern with the maximum reduction in sensitivity above the horizontal plane for a given sensor length occurs only at a single frequency which can be calculated. The equations derived were verified from directivity measurements made on several hydrophone sensors. They were found to be valid for all sensor lengths evaluated, piston dynamic mass ratios up to 2.55, and piston radii up to .159 times the wavelength.

NTIS
DDC
UNANNOUNCED
JUSTIFICATION
BY
DISTRIBUTION/AVAILABILITY CODES
Dist. AVAIL. and/or SPECIAL
A

Contents

HYDROPHONE SENSOR HAVING A CARDIOID DIRECTIVITY PATTERN

Introduction

To meet the demands for specialized underwater acoustic measurements by the Navy, the Underwater Sound Reference Division (USRD) of the Naval Research Laboratory is continually evaluating new hydrophone sensor configurations. These measurements often require hydrophones with unique directivity requirements.

The USRD was asked to develop a hydrophone having a directivity pattern within a limited frequency range that is omnidirectional in the space below its horizontal plane and with reduced sensitivity in the space above this plane. This requirement results in a hydrophone that is less sensitive to the interference of water surface reflections and acoustic noise due to sea state conditions. The hydrophone was also required to be omnidirectional in its horizontal plane.

The purpose of this report is to present an electroacoustic analysis and comparative performance of a hydrophone sensor configuration designed to fulfill this specific directivity need. Also, a design procedure is shown to configure a sensor of this type.

Scope And Approach

The scope of this report is based on a request for the USRD to develop a hydrophone having constant sensitivity at any angle below the horizontal plane and being optimized to have minimum sensitivity above this plane in the frequency range of 14.5 to 19.5 kHz.

The experimental evaluation of a known hydrophone sensor configuration having this directivity was completed. Various sensors based on this configuration were also experimentally evaluated. A concurrent electroacoustic analysis was initiated, and the resulting theoretical directivity was compared to the experimental. This was done so that an accurate design procedure could be developed for this sensor configuration to be applied to developing a sensor fulfilling the directivity specifications.

Results

Sensor Configuration

The sensor element configuration[1] analyzed is shown in Figure 1. It consists of an axially-poled piezoceramic tube with a concentric

- - - - -

[1]A. C. Tims and T. A. Henriquez, Patent No. 3,947,802, March 30, 1976.

Note: Manuscript submitted July 13, 1977.

circular piston cemented to each end. This assembly is sealed concentrically by O-rings inside a precision-bored, air-filled, tubular housing made of aluminum oxide. The O-rings provide a high-compliance suspension to the inner assembly to mechanically isolate and seal it inside the housing. The dielectric housing electrically insulates the pistons which act as electrodes for the piezoceramic tube. The housing also acoustically shields the inner assembly so that only the outside faces of the pistons are exposed to sound pressure. The sensor element in this hydrophone is mounted within an elastomer boot filled with castor oil.

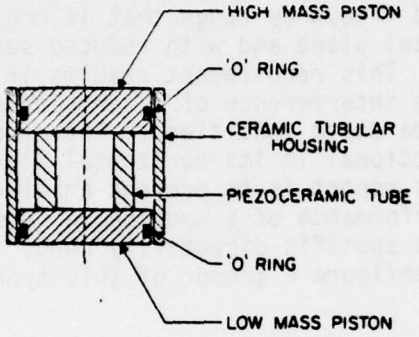

Fig. 1. Sensor element cross section

Others[2,3,4] reported on hydrophone sensors of this configuration but did not treat the directivity aspect of this design in the vertical plane.

Electromechanical Circuit Analysis

The physical parameters of the sensor configuration described are shown in Figure 2. When the piston surfaces are exposed to a sound field, the inner assembly vibrates about a nodal plane perpendicular to the piezoceramic tube axis.

- - - - -

[2]A. A. Aman'eva, Ceramic Acoustic Detectors (English translation published by Consultants Bureau Enterprises, Inc., New York, N. Y., 1956), Chapter 4, pp. 80-83.

[3]H. A. J. Rijnja, Acustica 30, 20-29 (1974).

[4]H. A. J. Rujnja, Acustica 33, 1-9, (1975).

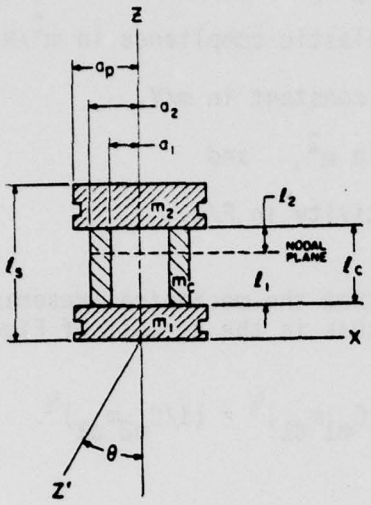

Fig. 2 ...nsor element physical parameters: m_1 is the small...on mass, m_2 the larger piston mass, and a_p the pis...adius; for the piezoceramic tube, m_c is its mass, ℓ_c its length, a_1 its inside radius, and a_2 its outside radius; ℓ_1 is the distance from the lower mass piston to the nodal plane, ℓ_2 the distance from the higher mass piston to the nodal plane, and ℓ_s the overall sensor length.

The electroacoustic equivalent circuit is shown in Figure 3, where the circuit parameters are identified, and is based on the following assumptions:

- That it operate below electroacoustic resonance where the sensor sensitivity is constant with frequency;
- that the acoustic radiation and mechanical resistances are negligible;
- that it operate at frequencies below the mechanical resonance of the pistons; and
- that for the piezoceramic tube

$$\phi = (s_{33}^D \ell_c)/(d_{33} S_c),$$

$$C_{m1} = s_{33}^D \ell_1 / S_c \text{ and } C_{m2} = s_{33}^D \ell_2 / S_c \qquad (1)$$

in m/N, and $C_e = \varepsilon_b S_c/\ell_c$ in F, where

s_{33}^D = open circuit elastic compliance in m^2/N,

d_{33} = piezoelectric constant in m/V,

$S_c = \pi(a_2^2 - a_1^2)$ in m^2, and

ε_b = blocked permitivity in F/m.

. Also, if we assume that the mechanical resonance frequency of the two mechanical branches in the circuit of Figure 3 are equal, then

$$\omega_o = (1/C_{m1}m_{d1})^{\frac{1}{2}} = (1/C_{m2}m_{d2})^{\frac{1}{2}}. \tag{2}$$

If

$$m_{d1} = m_1 + (m_c/3)\ (\ell_1/\ell_c), \tag{3}$$

$$m_{d2} = m_2 + (m_c/3)\ (\ell_2/\ell_c), \tag{4}$$

and

$$\ell_1 + \ell_2 = \ell_c, \tag{5}$$

substituting Eqs. (1), (3), (4), and (5) into Eq. (2) results in

$$m_{d1} = m_1 + \left(\frac{m_c}{3}\right)\left(\frac{m_2 + m_c/3}{m_1 + m_2 + 2m_c/3}\right) \tag{6}$$

and

$$m_{d2} = m_2 + \left(\frac{m_c}{3}\right)\left(\frac{m_1 + m_c/3}{m_1 + m_2\ 2m_c/3}\right). \tag{7}$$

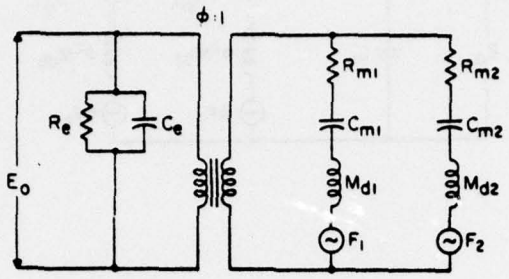

Fig. 3. Sensor electroacoustic equivalent circuit: C_e and R_e are the blocked electrical capacitance and resistance, ϕ is the voltage/force transduction ratio, R_{m1} and R_{m2} and C_{m1} and C_{m2} are the mechanical resistances and compliances of ℓ_1 and ℓ_2 respectively, m_{d1} and m_{d2} are the dynamic masses on either side of the nodal plane, F_1 and F_2 are force generators, and E_o is the open-circuit sensor voltage.

Figure 4 shows the electroacoustic equivalent circuit transformed to the equivalent electrical circuit and simplified by the foregoing assumptions. A network analysis by solving two simultaneous loop equations for Eo as a function of radian frequency ω gives

$$Eo = \phi F_1 \left\{ \frac{C_{m1}(1-\omega^2 C_{m2} m_{d2}) + C_{m2}\,(F_2/F_1)\,(1-\omega^2 C_{m1} m_{d1})}{C_{m1} + C_{m2} + \phi^2 C_e - \omega^2 C_{m1} C_{m2}(m_{d1} + m_{d2}) - \phi^2 \omega^2 C_e (C_{m2} m_{d2} + C_{m1} m_{d1} - \omega^2 C_{m1} C_{m2} m_{d1} m_{d2})} \right\} \quad (8)$$

where $\omega = 2\pi f$ in rad/sec and f = frequency in Hz.

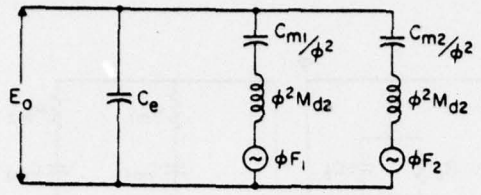

Fig. 4. Circuit of Fig. 3 transformed and simplified to give equivalent electrical circuit. Parameters same as Fig. 3

Theoretical Directivity

This hydrophone configuration is omnidirectional in the horizontal plane due to symmetry. F_1 and F_2 represent the amplitude of the pressure forces acting over the areas of pistons 1 and 2 caused by a plane acoustic wave traveling at angle θ as shown in Figure 2. Appendix A shows the derivation of the equations for these forces. Substitution of Eqs. (A11) and (A17) of Appendix A into Eq. (8) gives the open circuit voltage sensitivity of the sensor element for small ka_p in the vertical plane (x-z):

$$\frac{Eo}{p} = \left(\frac{\phi C_m S_p [D_m + \cos (k\ell_s \cos \theta)]}{(C_m + \phi^2 C_e)(D_m + 1) - \phi^2 \omega^2 C_e C_m m_{d2}} \right) \left(\frac{2J_1(ka_p \sin \theta)}{ka_p \sin \theta} \right) \qquad (9)$$

where $C_m = C_{m1} + C_{m2}$,

$S_p = \pi a_p^2$ in m^2 ,

$k = \omega/c = 2\pi/\lambda$,

c = sound velocity in m/sec ,

λ = wave length in m,

the dynamic mass ratio D_m is given by

$$D_m = \frac{m_{d2}}{m_{d1}} \quad , \qquad (10)$$

and $0 \leq \theta \leq 90^\circ$.

$J_1 (ka_p \sin \theta)$ represents the first order Bessel function of $ka_p \sin \theta$.

Eq. (9) reduces, for small values of ka_p and $k\ell_s$ to the familiar form

$$\frac{Eo}{p} = \frac{\phi C_m S_p}{C_m + \phi^2 C_e} .$$

The theoretical directivity of this sensor configuration in the vertical plane can be derived by taking the ratio of Eq. (9) evaluated at angle θ to that at $\theta = 0^\circ$. For $0 < \theta < 90^\circ$ one obtains

$$M_\theta = \left\{ \frac{D_m + \cos (k\ell_s \cos \theta)}{D_m + \cos (k\ell_s)} \right\} \left\{ \frac{2J_1 (ka_p \sin \theta)}{ka_p \sin \theta} \right\} \qquad (11)$$

where M_θ is the sensitivity ratio for the space below the x-y plane relative to that on the -Z axis. For the space above this plane, $90 \leq \theta \leq 180^\circ$, one obtains

$$M_\theta = \left\{ \frac{D_m \cos [k\ell_s \cos (180^\circ - \theta)] + 1}{D_m + \cos (k\ell_s)} \right\} \left\{ \frac{2J_1 [ka_p \sin (180^\circ - \theta)]}{ka_p \sin (180^\circ - \theta)} \right\} . \qquad (12)$$

From Eq. (12) it can be seen that for the maximum reduction in sensitivity above the x-y plane the numerator of the first term in brackets of Eq. (12) must be zero at $\theta = 180^\circ$. Then at this angle

$$D_m \cos (k\ell_s) + 1 = 0 ,$$

and solving for this value of $k\ell_s$

$$(k\ell_s)_0 = \text{Arcos } (-1/D_m). \qquad (13)$$

Examination of Eqs. (11) and (12) shows that the left term in brackets is a function only of D_m, $k\ell_s$, and θ. The right term in brackets is a function only of ka_p and θ. Note that this term is identical to the directivity term for a plane piston. Eq. (11) shows that for large values of D_m and small values of ka_p both terms in brackets approach unity and the sensor element will approach the omnidirective requirement in the space below the x-y plane (Figure 2).

Figures 5 and 6 are computer generated plots using Eqs. (11) and (12) in dB, showing the effect of D_m and ka_p on the directivity from $0^\circ \leq \theta \leq 180^\circ$ (x-z plane of Figure 2). Figure 5 shows the directivity

for values for D_m of 1 and 2.55 where $ka_p = .787$. For this plot $(k\ell_s)_0$ is calculated from Eq. (13) for each D_m. Figure 6 shows the directivity for $D_m = 2.55$ and values of ka_p of 0.1 and 1.0. This plot shows that there is very little effect of ka_p for values up 1.0. When ka_p becomes much greater than 1.0, Eqs. (11) and (12) become invalid because of assumption that $\lambda >> a_p$, for these equations (see Appendix A). The true cardioid directivity pattern occurs only at $(k\ell_s)_0$ as can be seen from these plots.

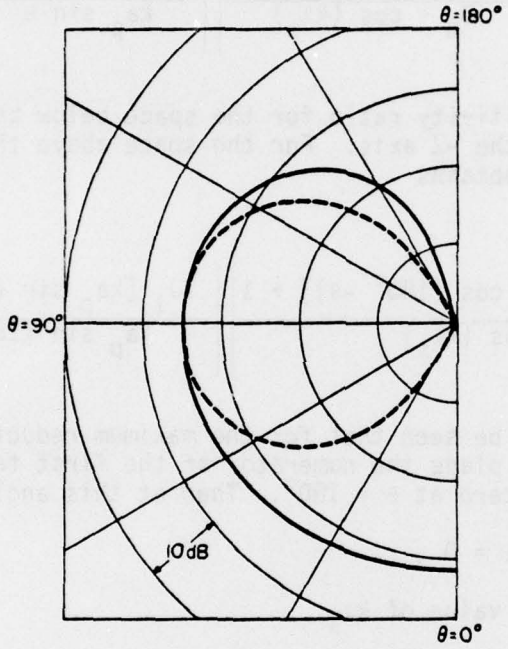

Fig. 5. X-Z directivity patterns of sensor element where $0° < \theta < 180°$ for $D_m = 1$ (dashed line) and $D_m = 2.55$ (solid line) calculated from Eqs. (11) and (12); $k\ell_s = (k\ell_s)_0$ calculated from Eq. (13) and $ka_p = 0.787$.

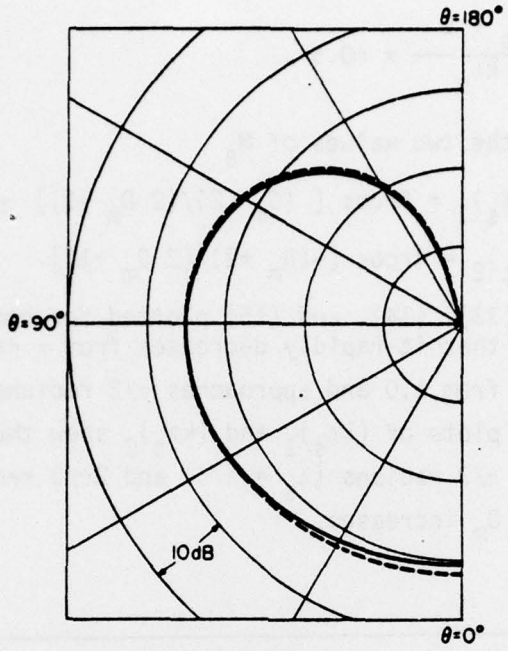

Fig. 6. X-Z directivity patterns of sensor element where $0° \leq \phi \leq 180°$ for $ka_p = 0.1$ (solid line) and $ka_p = 1.0$ (dashed line) calculated from Eqs. (11) and (12); $D_m = 2.55$ and $k\ell_s = (k\ell_s)_0$ calculated from Eq. (13).

These directivity patterns are shown only for $0° \leq \theta \leq 180°$ because for $180° \leq \theta \leq 360°$ the pattern is the mirror image of that shown. This is because the sensor is symmetrical in the x-z plane.

Consideration of Eq. (13) shows that $(k\ell_s)_0$ can have an infinite number of values but only the range of $\pi \leq (k\ell_s)_0 < \pi/2$ corresponding to $1 \leq D_m < \infty$ are of practical interest. Eq. (12) shows that the maximum reduction in sensitivity occurs at $\theta = 180°$ for any value of D_m. Also the sensitivity at $\theta = 180°$ increases as $k\ell_s$ changes in either direction from $(k\ell_s)_0$ within the above range. If $\theta = 180°$ and for small values

of ka_p where $\frac{2J_1(ka_p)}{ka_p} \simeq 1$, the values of $k\ell_s$ on either side of $(k\ell_s)_0$ can be found where $M_\theta \leq 0.5$ (-6 dB). For these conditions Eq. (12) becomes

$$M_\theta = \frac{D_m \cos k\ell_s + 1}{D_m + \cos k\ell_s} = \pm 0.5 \ .$$

Solving for $k\ell_s$ for the two values of M_θ

$$(k\ell_s)_1 = \text{Arcos}\ [\ (D_m - 2)/(2\ D_m + 1)] \text{ and} \qquad (14)$$

$$(k\ell_s)_2 = \text{Arcos}\ [-(D_m + 2)/(2\ D_m + 1)]. \qquad (15)$$

Figure 7 shows Eqs. (13), (14), and (15) plotted for comparison. The plot of $(k\ell_s)_0$ shows that it rapidly decreases from π radians ($\ell_s = \lambda/2$) as D_m increases from 1.0 and approaches $\pi/2$ radians ($\ell_s = \lambda/4$) asymptotically. The plots of $(k\ell_s)_1$ and $(k\ell_s)_2$ show the same trend except they approach $\pi/3$ radians ($\ell_s = \lambda/6$) and $2\pi/3$ radians ($\ell_s = \lambda/3$) respectively as D_m increases.

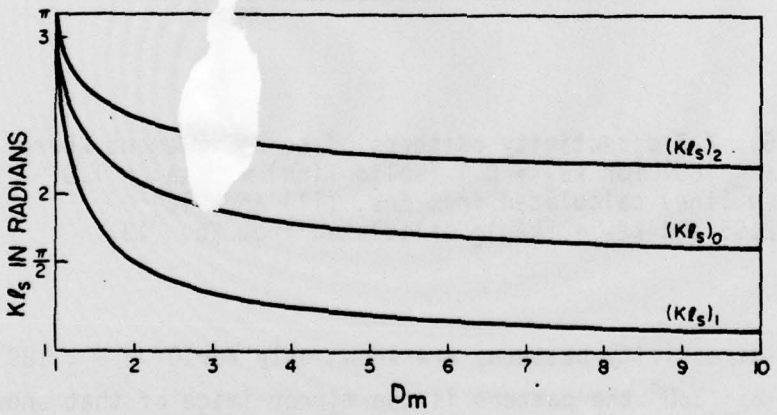

Fig. 7. Plots of Eqs. (13), (14), and (15). The area bounded by the curves for $(k\ell_s)_1$ and $(k\ell_s)_2$ contain all values for $k\ell_s$ and D_m where $M_\theta \leq 0.5$ (-6 dB) at $\theta = 180°$.

Experimental Directivity Comparison

The validity of the theoretical directivity developed for this sensor configuration was verified by computer generated directivity

patterns of the USRD type H56 hydrophone using Eqs. (11) and (12). Comparison of these theoretical plots with the actual directivity measured at the USRD Lake Facility is shown in Figures 8a thru c for three frequencies. The center frequency of 27 kHz was calculated from Eq. (13) where for this hydrophone D_m = 2.46, the sensor length ℓ_s = 17.45 mm, and a_p = 7.87 mm. The plots show good agreement between measured and calculated plots. The worst agreement shown was for a frequency of 30 kHz. This can be attributed to diffraction due to proximity of the hydrophone preamplifier housing at the top and the sensor frame ring at the bottom of the pattern and the fact that at this frequency ka_p is almost 1.0.

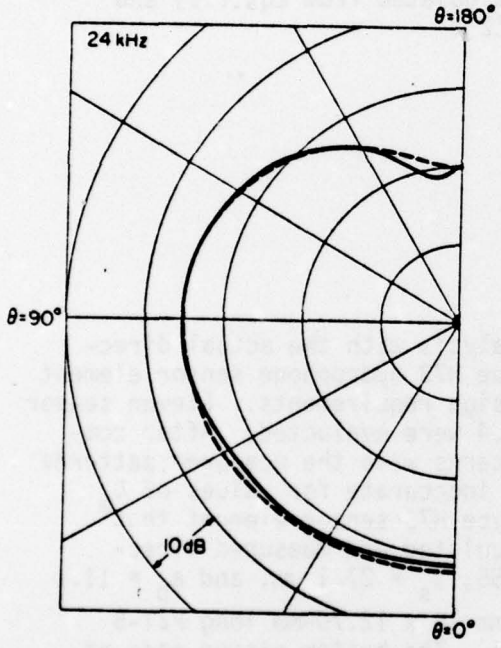

Fig. 8a

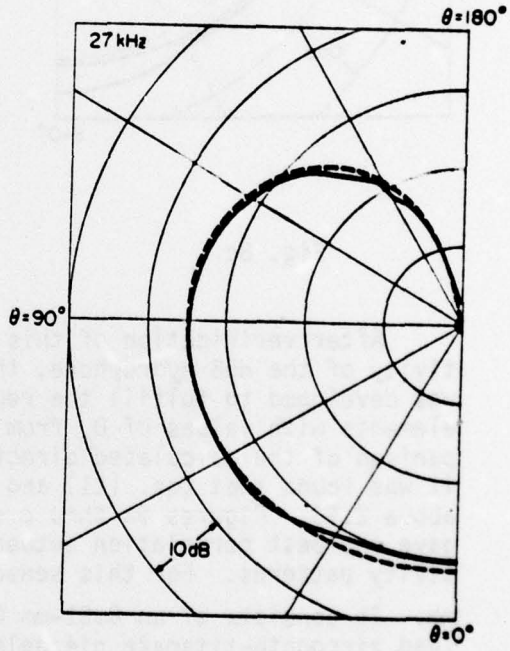

Fig. 8b

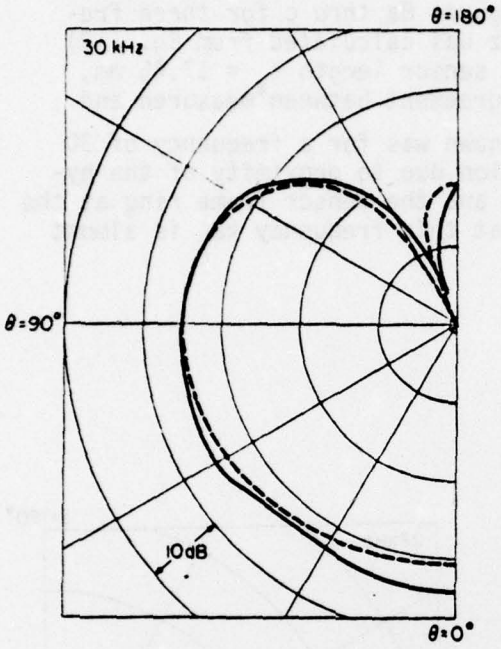

Figs. 8a-c. X-Z directivity patterns for USRD type H56 hydrophone where $0^\circ \leq \theta \leq 180^\circ$ for 3 frequencies shown; solid lines are measured patterns and dashed lines are patterns calculated from Eqs.(11) and (12).

Fig. 8c

After verification of this design analysis with the actual directivity of the H56 hydrophone, the USRD type H73 hydrophone sensor element was developed to fulfill the requested design requirements. Eleven sensor elements with values of D_m from 1.8 to 10.4 were evaluated. After comparison of the calculated directivity patterns with the measured patterns it was found that Eqs. (11) and (12) were inaccurate for values of D_m above 2.55. Figures 9a thru c show the type H73 sensor element that gave the best correlation between the calculated and measured directivity patterns. For this sensor $D_m = 2.55$, $\ell_s = 27.1$ mm, and $a_p = 11.1$ mm. It consists of an 8.51-mm OD x 5.02-mm ID x 12.70-mm long PZT-5 lead zirconate-titanate piezoelectric tube. The bottom piston made of type 6061-T6 aluminum alloy is 6.35-mm thick and has a mass of 6.11 g. The top piston, made of type 304 stainless steel, is 8.05-mm thick and has a mass of 23.05 g.

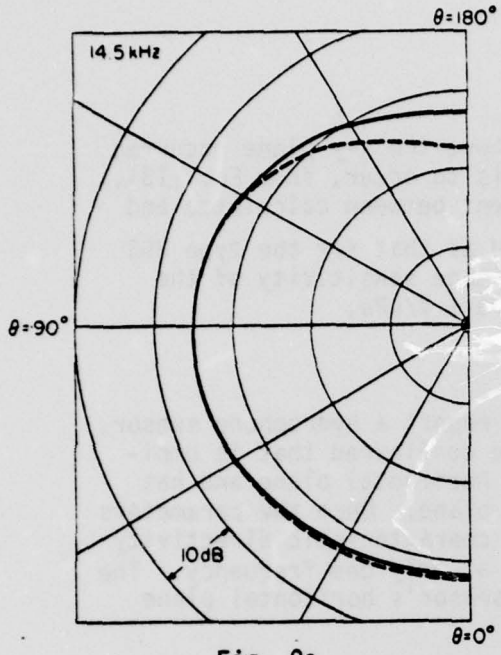

Fig. 9a

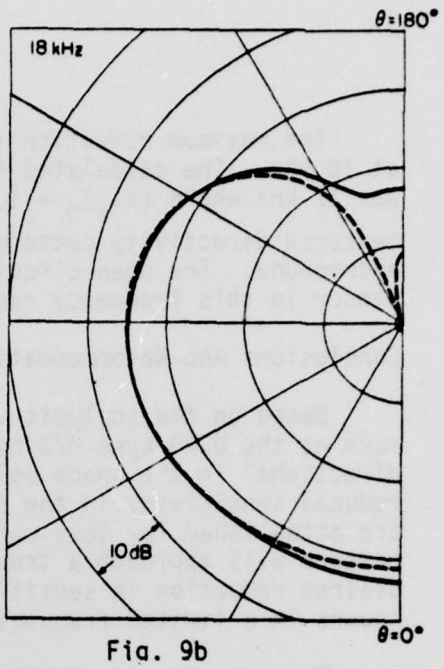

Fig. 9b

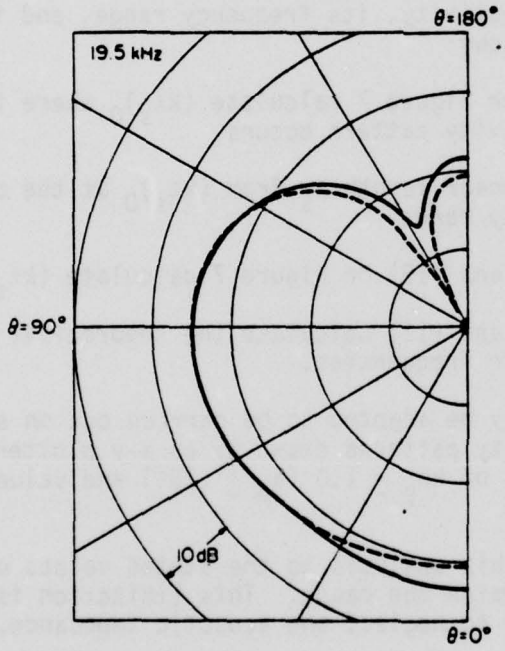

Fig. 9c

Fig. 9a-c. X-Z directivity patterns for USRD type H73 hydrophone where $0^\circ < \theta < 180^\circ$ for 3 frequencies shown; solid lines are measured patterns and dashed lines are patterns calculated from Eqs. (11) and (12).

The maximum reduction in sensitivity above the x-y plane occurred at 18 kHz. The calculated frequency for this to occur, from Eq. (13), was 17 kHz where $(k\ell_s)_0 = 1.97$. The agreement between calculated and measured directivity patterns is not as good as that for the type H56 hydrophone. The open-circuit free-field voltage sensitivity of the sensor in this frequency range was -182 dB re 1 V/μPa.

Conclusions And Recommendations

Based on the analysis verified in this report a hydrophone sensor, such as the USRD type H73 hydrophone, can be configured that is omnidirectional in the space below the sensor's horizontal plane and has reduced sensitivity in the space above this plane. Once the parameters are established for this configuration, its characteristic directivity pattern will approach a true cardioid shape at only one frequency. The desired reduction in sensitivity above the sensor's horizontal plane occurs in a limited frequency range.

The procedure in designing a sensor element of this configuration knowing its desired directivity, its frequency range, and its dynamic mass ratio D_m is as follows:

1) Using Eq. (13) or Figure 7 calculate $(k\ell_s)_0$ where the theoretical cardioid directivity pattern occurs.

2) Calculate the sensor length ℓ_s from $(k\ell_s)_0$ at the center of the desired frequency range.

3) Using Eqs. (14) and (15) or Figure 7 calculate $(k\ell_s)_1$ and $(k\ell_s)_2$.

4) Using Eqs. (11) and (12) calculate the theoretical directivity patterns at other frequencies.

This procedure can easily be adapted to be carried out on a digital computer with the directivity patterns drawn by an x-y plotter. This analysis is valid for values of $ka_p \leq 1.0$ ($a_p \leq .16\lambda$) and values of dynamic mass ratio $D_m \leq 2.55$.

The limitation of this analysis to the stated values of D_m should be investigated to determine the cause. This limitation is probably caused by the assumption to neglect the acoustic impedance.

Acknowledgments

The author wishes to thank Allan C. Tims of the USRD for his work in fabrication and design of the experimental hydrophones and Theodore A. Henriquez of the USRD for his help in the acoustic analysis.

APPENDIX: WAVE ANALYSIS

The forces F_1 and F_2 in Eq. (8) represent the force amplitudes caused by the sound pressure acting on pistons 1 and 2 (represented by masses m_1 and m_2 in Figure 2). The force on piston 1 for $\lambda >> a_p$ is given by the equation

$$F_1(\theta,t) = 4\int_0^{a_p} p_1(x,\theta,t)\, y\, dx \qquad (A1)$$

where $p_1(x,\theta,t)$ is the sound pressure distribution on the piston and $y\,dx$ is the differential area over which $p_1(x,\theta,t)$ acts at any coordinate x.

The plane wave equation on the Z' axis is

$$p(z',t) = p_p(\cos \omega t)(\cos kz') \qquad (A2)$$

where p_p is the sound pressure amplitude, ω and k are as defined before, and z' is the distance from the origin. For any coordinate x on piston 1 the corresponding coordinate along the Z' axis (Figure 1A) is

$$z' = x \sin \theta. \qquad (A3)$$

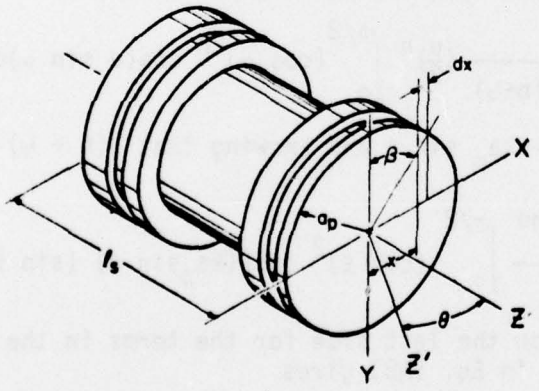

Fig. 1A. Coordinate system for sensor looking at piston 1.

Substituting Eq. (A3) in Eq. (A2) gives

$$p_1(x,\theta,t) = p_p(\cos \omega t)\,[\cos(k\, x \sin \theta)]. \qquad (A4)$$

Looking at Figure 1A, it can be seen that

$$y = (a_p^2 - x^2)^{\frac{1}{2}}$$

and therefore

$$ydx = (a_p^2 - x^2)^{\frac{1}{2}}\, dx. \tag{A5}$$

Also note from Figure 1A

$$x = a_p \sin \beta \text{ and } dx = a_p \cos \beta d\beta. \tag{A6}$$

Substituting Eq. (A6) into Eqs. (A4) and (A5) gives

$$p_1(x,\theta,t) = p_1(\beta,\theta,t) = p_p(\cos \omega t)\cos[(ka_p \sin \theta)(\sin \beta)], \text{ and}$$
$$ydx = a_p^2 (\cos \beta)^2\, d\beta. \tag{A7}$$

Substituting Eq. (A7) into Eq. (A1) gives the final transformation to polar form

$$F_1(\theta,t) = 4p_p a_p^2 \cos \omega t \int_o^{\pi/2} (\cos \beta)^2 \cos[(ka_p \sin \theta)(\sin \beta)]\, d\beta. \tag{A8}$$

From Reference 5 the following definite integral expression for a Bessel Function of order n where $n > -\frac{1}{2}$ is given as

$$J_n(u) = \frac{2}{\sqrt{\pi} \cdot \Gamma(n+\frac{1}{2})} \left(\frac{u}{2}\right)^n \int_o^{\pi/2} (\cos \alpha)^{2n} \cos(u \sin \alpha) d\alpha. \tag{A9}$$

If $n = 1$, $\alpha = \beta$ and $u = ka_p \sin \theta$ and knowing that $\Gamma(n + \frac{1}{2}) = \pi/2$ Eq. (A9) becomes

$$J_1(ka_p \sin\theta) = \frac{2ka_p \sin\theta}{\pi} \int_o^{\pi/2} (\cos \beta)^2 \cos[(ka_p \sin \theta)(\sin \beta)] d\beta. \tag{A10}$$

Substituting the term on the left side for the terms in the right side of Eq. (A10) contained in Eq. (A8) gives

$$F_1(\theta,t) = p_p S_p \cos \omega t \left(\frac{2J_1 (ka_p \sin \theta)}{ka_p \sin \theta} \right)$$

---

[5] T. M. McRoberts, Spherical Harmonics (Dover Publications, Inc., New York, N.Y., 1947) Chap. 14, pp 255-257.

where $S_p = \pi a_p^2$, the piston area.

Finally, the amplitude of $F_1(\theta,t)$ is

$$F_1 = p_p S_p \left| \frac{2J_1 (ka_p \sin\theta)}{ka_p \sin\theta} \right| . \qquad (A11)$$

The force on piston 2, for $\lambda >> a_p$ is given by

$$F_2(\theta,t) = 4 \int_o^{a_p} p_2(x,\theta,t) y dx \qquad (A12)$$

where $p_2(x,\theta,t)$ is the sound pressure distribution on this piston and ydx is differential area over which $p_2(x,\theta,t)$ acts at any coordinate x. For any coordinate x in piston 2 the corresponding coordinate along the Z' axis (Figure 1A) is

$$z' = \ell_s \cos\theta + x \sin\theta. \qquad (A13)$$

Substituting Eq. (A13) in Eq. (A2) gives

$$p_2(x,\theta,t) = p_p(\cos\omega t) \cos[k(\ell_s \cos\theta + x \sin\theta)]. \qquad (A14)$$

Transforming Eq. (A14) and by substituting for x from Eq. (A6) gives

$$p_2(x,\theta,t) = p_2(\beta,\theta,t) = p_p(\cos\omega t)\cos\{k[\ell_s \cos\theta - a_p(\sin\theta)(\sin\beta)]\}. \qquad (A15)$$

Substituting Eq. (A15) and with the area ydx from Eq. (A7), Eq. (A12) becomes

$$F_2(\theta,t) = 4p_p a_p^2 \cos\omega t \int_o^{\pi/2} (\cos\beta)^2 \cos\{k[\ell_s \cos\theta + a_p(\sin\theta)(\sin\beta)]\} d\beta.$$

This equation, using a trigonometric identity, becomes

$$F_2(\theta,t) = 4p_p a_p^2 (\cos\omega t)[\cos(k\ell_s \cos\theta)] \int_o^{\pi/2} (\cos\beta)^2 \cos[ka_p(\sin\theta)(\sin\beta)] d\beta$$

$$-4p_p a_p^2 (\cos\omega t)[\sin(k\ell_s \cos\theta)] \int_o^{\pi/2} (\cos\beta)^2 \sin[ka_p(\sin\theta)(\sin\beta)] d\beta. \qquad (A16)$$

The second term of Eq. (A16) when integrated is zero. Finally, the first

term in Eq. (A16), after rearranging to the form of Eq. (A10), gives

$$F_2(\theta,t) = p_p S_p (\cos\omega t)[\cos(k\ell_s \cos\theta)]\left\{\frac{2J_1 (ka_p \sin\theta)}{ka_p \sin\theta}\right\}$$

and the amplitude of $F_2(\theta,t)$ is

$$F_2 = p_p S_p [\cos (k\ell_s \cos\theta)] \left\{\frac{2J_1 (ka_p \sin\theta)}{ka_p \sin\theta}\right\}. \qquad \text{(A17)}$$